www.czasopisma.pan.pl PAN POLSKA AKADEMIA NAUK www.journals.pan.pl

Arch. Metall. Mater. **65** (2020), 2, 697-705

DOI: 10.24425/amm.2020.132808

K. JAŚKIEWICZ[1], M. SKWARSKI[1*], S. POLAK[1], Z. GRONOSTAJSKI[1],
J. KRAWCZYK[1], P. KACZYŃSKI[1], W. CHORZĘPA[2]

ANALYSIS OF THE FORMING PROCESS OF ENERGY-ABSORBING ELEMENTS MADE FROM 7000 SERIES HIGH-STRENGTH ALUMINUM ALLOY

The paper covers the research on the process of solutionizing of 7075 aluminum alloy in cold tools during the stamping of a high-strength structural element (B-pillar's base). For technological reasons, in order to obtain high strength parameters of the 7075 alloy, it is necessary to carry out a solutionization process, which allows to obtain dispersion strengthening during ageing process. Properly performed heat treatment of the alloy increases the strength of the material to approx. 600 MPa. The combination of the process of solutionization with simultaneous shaping is aimed at improving and simplifying technological operations of aluminum alloy stamping, shortening the duration of the manufacturing process and reducing production costs. The manufactured lower part of the B-pillar will be used for the verification of the validity of the developed method. During the experiment, a series of stamping tests were carried out, in which the lubricants, pressure and position of the upper and lower blankholders were the variables. The obtained results allow to estimate the influence of the cooling conditions on the strength of the drawpieces obtained after the process of artificial ageing. In order to verify and analyse the results more quickly, a numerical simulation was carried out.

Keywords: aluminum alloys, hot forming

1. Introduction

European environmental requirements impose limits on the fuel consumption and exhaust emissions of modern cars. One way to meet the requirements is to replace the rigid, steel structural parts of the car body with light metal alloys, which are less dense and have higher strength at the same time. Currently, the greatest potential among light metal alloys in this area is represented by the 6000 and 7000 aluminum alloy series for plastic forming [1,2]. This material, which is more than three times lighter than steel, is characterized by very high strength after heat treatment (in T6 strengthened temper). After the process of solutionization and artificial ageing its maximum tensile strength can reach 650 MPa. However, due to very low strain in T6 or T4 temper, stamping at ambient temperature complex shapes of car body parts is almost impossible. Therefore, the material should be prior subjected to heat treatment in order to increase its plastic properties or a hot forming process at an elevated temperature should be applied, which allows the material to achieve high deformability without significant loss of the strength [3-5].

5000, 6000 and 7000 aluminum alloys have great potential for hot forming due to their good plastic properties (tensile strain can reach up to 0,6). As the material is heated, the yield stress decreases and the grain size of the material changes, which affects the final strength, which is related to the phenomenon of thermally activated dislocation lines [6]. LDR and LDH tests have demonstrated that 7075 aluminum alloy is susceptible to deep drawing processing when heated to temperatures in the range of 140-220°C. Heating up the material to a temperature above 260°C results in microstructural changes, which reduces its mechanical properties [7]. Additionally there are also a research into properties improvement of aluminum alloys by microstructure refinement [8]. One of the most beneficial initial temper of the material in terms of hot forming processes is T1 temper, especially at high deformation rates. The forming temperature of 250°C dissolves metastable precipitates. The short exposure of about 30 s at 250°C and subsequent precipitation strengthening by natural ageing combined with the paint bake cycle restores the hardness level of T6 temper [9]. It was demonstrated that it is possible to warm stamp elements of complex geometry, like the car's bracket [10] and B-pillar [11] out of 7075 aluminum alloys.

[1] WROCLAW UNIVERSITY OF SCIENCE AND TECHNOLOGY, FACULTY OF MECHANICAL ENGINEERING, 27 WYBRZEŻE ST. WYSPIAŃSKIEGO STR., 50-370 WROCŁAW, POLAND
[2] KIRCHHOFF POLSKA SP. Z O.O., WOJSKA POLSKIEGO STR., 339-300 MIELEC, POLAND

* Corresponding author: mateusz.skwarski@pwr.edu.pl

The final geometry was free from cracks and galling of the material thanks to the appropriate modification of the warm forming parameters. However, the high strength properties of the finished product were not achieved. In addition, the geometry of the finished part should be within the acceptable shape deviations. This goal is difficult to achieve due to the increased spring-back of the material deformed at elevated temperatures. The springing of the material can be 10% smaller under non-isothermal shaping conditions compared to isothermal conditions [12,13]. The springing is additionally affected by the strain rate. Increased velocity of the punch results in beneficial forming conditions due to the lower dynamic recovery, which affects the stability of deformation and springing [14]. The heat transfer between the workpiece and the forming tools is another important aspect. The main parameters describing this quantity are the conductive heat transfer coefficient and the heat transfer coefficient. Both of the described quantities are necessary for FEM modeling of the warm forming processes [15]. The performed simulations clearly prooves that greater deformability of aluminum alloys can be obtained by heating the edges and core of the punch and matrix to varying temperatures [16].

The second technology for forming hard-deformable aluminum alloys is hot forming. The first attempts of the hot forming of aluminum alloys were made as early as in the 1990s. Evangelista et al. investigated the possibility of using a 6061 aluminum alloy for hot stamping technology [17]. The material's formability was tested by torsion tests conducted in the temperature range from 250 to 500°C. It was demonstrated that the high potential of the material for hot pressing results from the microstructural changes occurring at elevated temperatures as well as from dynamic healing. Cavaliere (2002) conducted similar tests on 2618 aluminum alloy observing precipitation hardening during material deformation. Additionally, the influence of hardening phases on the stress-strain curves was determined [18]. The microstructure and distribution of precipitates of 2000 series aluminum alloys after the quenching in water was carried out by the Barenji et al. [19]. A similar analysis of 6000 series alloys was conducted by Fan et al. [20].

Providing the material of a high strength (like precipitation hardening 2000, 6000 and 7000 aluminum alloys) and increased plastic properties is achieved by removing the T6 temper prior to forming operation and subsequent artificial ageing after stamping [21]. For this purpose, the input material is heated up to the temperature of about 500°C and hold for the time needed to obtain a homogeneous solution in which the precipitates, phases and strengthening particles are dissolved into an Al-rich solid matrix [22]. This increases the plasticity of the material to a large extent, enabling a complex geometry to be obtained during the stamping process without losing stability. After holding for a proper amount of time the hot blank should be immediately transferred and formed by tools having a temperature low enough to cool down the material at the right rate below the temperature corresponding to the limit point of maximum solubility. In this process, the material is both solutionized and shaped accordingly [23]. The tools exerting pressure on the deformed material dissipate the heat from the blank so quickly that it causes freezing of the solutionized state in the material, which according to the equilibrium diagram does not occur at ambient temperature [24,25]. The solutionized state is necessary for further heat treatment, i.e. artificial ageing, during which particles and phases strongly strengthening the material are precipitated. This results in the restoration of very high strength and hardness [26].

Tensile and structural tests of the material after thermo-plastic treatment have proved that the two main factors influencing the strength and microstructure of the final product includes: transferring the material from the furnace to the tools and the cooling fluid. The effect of solutionization temperature and the cooling rate on the type, size and density of strengthening particles have been extensively tested for 7000 [27,28] aluminum alloys series and 6000 [29].

The practical application of aluminum hot forming technology (e.g. manufacturing a B-pillar from 7075 series aluminum alloy) is associated with the need to overcome many technological problems, including reduced strength properties, material folding and loss of stability [30]. The most important parameters of thermo-plastic treatment include time, temperature as well as the heating and cooling rate. The heating rate directly affects the dissolution kinetics and significantly shortens the soaking time [31]. The solutionization temperature does not affect the alloy's deformability, but it can have a significant impact on the strength properties of the final product. The emerging defects in the form of loss of stability and large galling areas result from a lack of lubrication as well as from uneven material temperature and the uneven cooling rate at the forming stage. Obtaining the hot-formed B-pillar from 7075 aluminum alloy without defects is possible on condition that a proper lubricant is used, e.g. graphite suspension or molybdenum disulphide. It doesn't matter if the grease will be applied to the surface of the sheet or to the surface of the tools. In order to shorten the manufacturing process, Zhou et al. attempted to combine the artificial aging process with painting the drawpiece. This resulted in high strength properties of the finished product, despite a significant reduction in soaking time. Optimization of the process parameters, such as the clamping force, type of tools' lubricant or time of transfer of the blank from the furnace to the stamping station, which directly affects the temperature of the input, allows to obtain the drawpieces of a complex geometry [32].

Preliminary studies on the formability of aluminum alloys allowed to determine material parameters such as press-formability and stress-strain curves in various conditions [33,34]. The use of digital image correlation allowed to determine the actual stress-strain curves and to determine the material's sensitivity to the strain rate at high temperatures [35]. In order to develop two strain rate dependent material models, the Nakajima tests have been conducted at elevated temperatures [12]. The hot forming results in the change of the temperature of the material during the process, which directly affects the thermal and mechanical properties of the material. The sheet metal made of 7075 aluminum alloy was comprehensively examined using a 3500 Gleeble thermo-mechanical testing system [36]. The

influence of the forming speed on the material temperature was determined. Additionally, extensive microstructural tests were conducted. In consequence 7075 aluminum alloy processing maps, taking into account the phenomenon of dynamic healing and dynamic recrystallization were created. Song et al. examined the influence of the stamp velocity on the shape of the hot-formed, thin-walled, cylindrical elements made of 7075 aluminum alloy. This allowed determining the input data for FE modeling which resulted in obtaining the distribution of material thickness and temperature [37].

Another significant obstacle occurring the during forming of aluminum alloys at elevated temperatures is the phenomenon of material galling and the formation of built-up on the surface of tools. This phenomenon is caused by the increase in tools-to-material friction coefficient in comparison to cold forming. Research on the 5182 aluminum alloy galling during the hot forming processes was carried out by Riahi and Alpas [38]. The tests were carried out using aluminum sheets of room temperature and heated up to 420°C. Three types of cold tools made of AISI 52100 steel were tested: uncoated, DLC coated and unhydrogenated TiN coated. Independently of the blanks' temperature, the DLC coating provided the lowest material galling in comparison with uncoated and TiN coated tools. Dong and his team tested carbon and plasma nitrided CAPVD WC: C. coatings. The results show that coating reduced the aluminium sticking on the tool surfaces, to the extent that it achieved an 80% lubricant reduction in the hot forming [39].

Simulating the hot forming of aluminum alloys is a big challenge in the scientific community. Accurate reproduction of material properties is a very difficult task. This is mainly caused by the variable nature of the process – the temperature of the material and tools change over time, and thus their mechanical properties change as well. On the basis of simple solutionization tests, the authors of the publication [40] estimated the thermal contact conductance. The rest of the parameters needed to conduct FE simulation were adopted from the ESi software database. Due to the lack of data related to the anisotropy of the material at elevated temperatures, thinning in the biaxial tension area was underestimated. The reason for this state is that the isotropic model overestimates the ratio of in-plane deformation to out-of-plane deformation [41]. On the basis of conducted simulations, it was concluded that the required cooling time needed to obtain full solutionization of the material is very short in comparison to the cooling time of steel elements. This is caused by the coincidence of several factors: 1) the solutionization temperature of the aluminum equals half the quenching temperature of the steel elements (T_{AL} = ½ T_{ST}); 2) the density of aluminum is one-quarter of the density of steel (ρ_{AL} = ¼ ρ_{ST}); 3) The specific heat capacity of aluminum alloys is less than that of steel (λ_{AL} = 0,68 x λ_{ST}). Taking all these factors into consideration the amount of energy to be removed from the aluminum blank equals half of the energy accumulated in the steel blank of the same thickness (E_{AL} = ½ E_{ST}). The temperature of the aluminum sheet after solutionization is more homogeneous because aluminum has 4 times higher thermal conductivity. The conclusions drawn from the aftermentioned publication were taken into account during the FE simulation of the hot forming process. Simulations carried out by Liu et al. proved that the higher the strain rate, the more even the distribution of material wall thickness. Thanks to the tools proposed by Li, it is not necessary to measure the hardness of the material after heat treatment, as the numerical simulation is sufficient to estimate the value of the hardness of the material depending on the process parameters, without destructive testing [42].

The aim of the authors was to produce a drawpiece of a complex geometry, which is the lower part (base) of the B-pillar in the hot forming process from a high strength 7075 series aluminum alloy. A properly made drawpiece should not have any geometric defects in the form of narrowing, thinning, cracks, folds or large scratches. For practical reasons, the development of the process was carried out taking into consideration the possibility of its application in the automotive industry. Therefore, technological complexity and production costs were taken into consideration.

2. The subject of the study

The subject of the study was 7075, T6 temper aluminum alloy in the form of a 3 mm thick sheets. The material at room temperature has the ultimate tensile strength (Rm) equal to 600 MPa and hardness at the level of 195 HV1. According to the certificate provided by the manufacturer, the aluminum alloy had the chemical composition shown in Table 1.

TABLE 1

Chemical composition of the tested 7075 aluminum alloy

Alloy addition	Si	Fe	Cu	Mn	Mg	Cr	Zn	Ti	Ti+Zr	Others
Content %	0,06	0,12	1,6	0,02	2,6	0,19	5,8	0,05	0,08	0,02

3. Research methodology

Experimental tests were carried out with the use of a stamping die (Fig. 1a) designed and manufactured by Kirchhoff Poland in Mielec. The tools were installed on a 2000 kN hydraulic press. The tools' material is 1.2738HH improved alloy steel of very good surface quality, low thermal expansion and high resistance to temperature changes. The stamping tools were used to produce the base of the car's B-pillar, shown in Fig. 1b.

The production of the tested element started with heating the blank that was cut out beforehand from the 3 mm thick 7075 aluminum sheet. The input was heated up to 480°C and held for 60 minutes to dissolve phases and particles. Next, the blank was immediately transported to cold tools and the forming process was started. The stamping process was initiated by pushing out the movable lower blankholder (4) by means of a hydraulic cushion of the press to the height of the upper surface

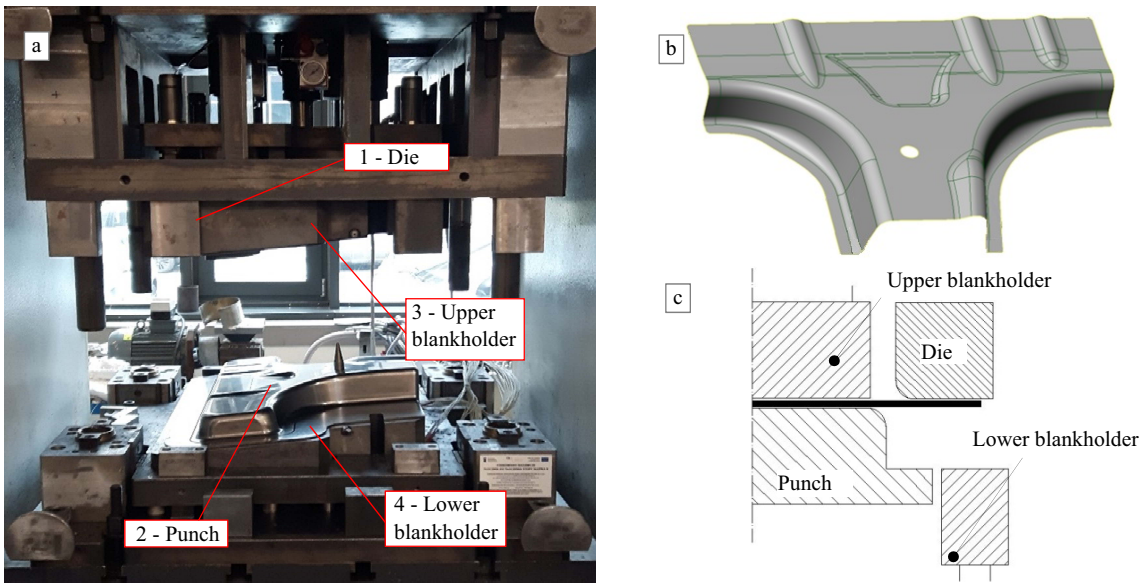

Fig. 1. a) Tools for stamping of the base of B-pillar, b) CAD model of the B-pillar base, c) Position of the shaping tools and blankholders

of the punch (2), so that they would form a common surface. After the press was started, the die (1) and the upper blankholder (3) were moved down until the first contact with the material occurred. Secondly, the further movement of the die caused the sheet metal to press on the lower blankholder and after exceeding the preset pressure, the product was shaped on a stationary punch (2). The diagram showing the configuration of the tools is shown in Fig. 1c. The auxiliary elements of the tools in the form of blankholders are the first to come into contact with the hot blank and affect its cooling speed. Therefore, a very important aspect during the forming process is setting their parameters, such as pressure or initial position.

Some of the drawpieces were tested for corrosion resistance (the test was carried out in Kirchoff company). The experiment included double degreasing of products, activation, zinc phosphating, cataphoretic painting, during which the samples were treated with KTL coating, multi-stage rinsing and drying. The samples prepared in this way were subjected to CASS corrosion (tests in hydrochloric mist atmosphere in the presence of copper chloride and acetic acid). Table 2 presents operating conditions of the chamber according to AA-0129 3.2.4. The prepared samples were scratched in accordance with BMW GS 90011:2014-02; PN-EN ISO 9227:2012; AA-0129:2015-04; AA 0169:2010-05 standards. The samples prepared in this way were tested for 144 hours. Coatings applied on the surface of the drawpieces were checked for: coating thickness, adhesion forces of the coating to the metal sheet, the occurrence of corrosion bubbles and average delamination width of the coating.

In the next step, the finished drawpieces were scanned with a contactless method using the ROMER 7520si measuring arm equipped with an integrated RS3 scanner. Thanks to this, it was possible to determine the distribution of the material thickness reduction on the drawpiece. The thickness reduction of the drawpiece was additionally determined using the FEM method which takes the actual stamping conditions into consideration. The numerical FE model (Fig. 2) consisted of the material being formed (5), a punch (2), a die (1), a lower blankholder (4) and an upper blankholder (3). The parameters of the process are presented in Table 3.

TABLE 2

Corrosion resistance test parameters

Temperature	49-50°C
pH	3,25
Concentration of sodium chloride	5%
Avarage wear rate	80 cm^3 = 1,49 ml/h
Concentration of copper chloride II	0,249 g/l
Device	606 Erichsen (Basic 400) salt spray chamber

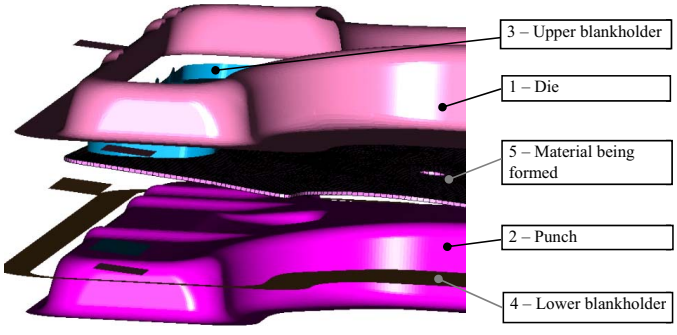

Fig. 2. FE model of stamping of the B-pillar's base

The material model was built in the form of points. It is strain, strain rate and temperature dependent ($\sigma(\varepsilon, \dot{\varepsilon}, T)$). Materials were validated for temperatures of 21, 100, 200, 230, 300, 350, 400, 420 and 500°C, for strain rate equal to 0.001, 0.01 and 0.1 s^{-1}. The results of the analysis were extrapolated in the Matlab software for higher strain rates and deformation levels. The material model was adopted as isotropic.

TABLE 3

Parameters of the stamping process taken into consideration in numerical simulation

Temperature of the input before stamping	480°C
Temperature of the tools	21°C
Pressure on the counterpunch (upper blankholder)	5 bar (increases to 15 bar at the end of the process)
Pressure on the cushion (lower blankholder)	30 bar (remains constant till the end of the process)
Height (position) of the lower blankholder according to Fig. 2	0, 11, 21, 31 mm

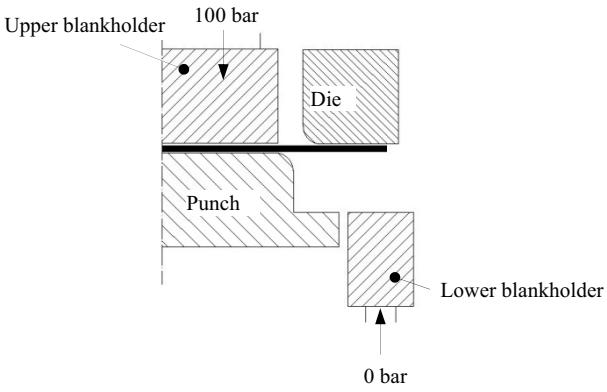

Fig. 3. Forming parameters and tools' setting

4. Results

The preliminary tests were carried out for the pressure of the upper blankholder equal to 100 bar and pressure of the lower blankholder equal to 0 bar. The stamping tests were performed with Setol 356 oil as well as with graphite + water mixture. Lubricants were applied only to the surface of the tools. Additionally, in cases when the blank was cracking, the blank was covered with lubricant. In the preliminary tests, the lower blankholder was located outside the stamping zone and did not take part in the process (Fig. 3).

During the tests conducted with the use of Setol 356 (for hot pressing) the material cracked in areas 1 and 2 and delaminated strongly in area 3 (Fig. 4a). Numerical simulations have shown that areas 1 and 2 will have the highest strain concentration, which induces a risk of stability loss (Fig. 13). In order to further reduce the coefficient of friction between hot material and cold tools, another test was carried out with a blank, on which a layer of Setol 356 oil was additionally applied before heating. This time, the loss of continuity of the material occurred only in area 3 shown in Fig. 4b. As a result of the heating of the drawpiece in a furnace, the oil burnt and a thin, hardly removable, dark layer remained stick to the drawpiece. During subsequent forming

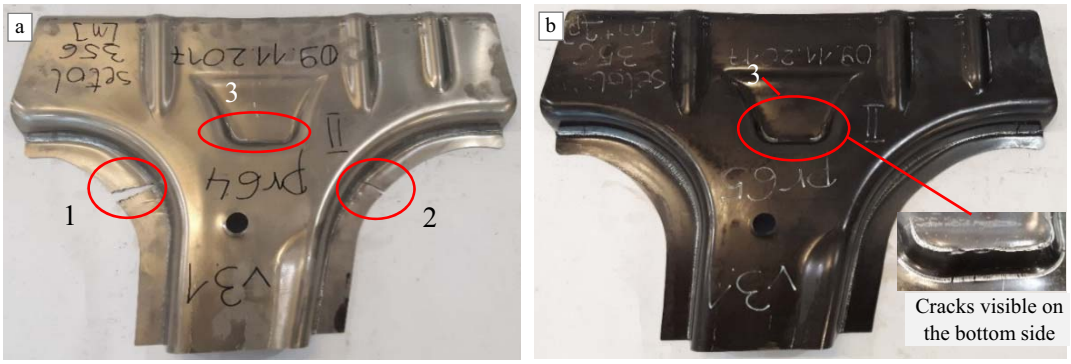

Fig. 4. Forming tests conducted with the use of Setol 356 oil, test parameters according to Fig. 3; a) lubrication of the tools only, b) lubrication of the tools and the blank

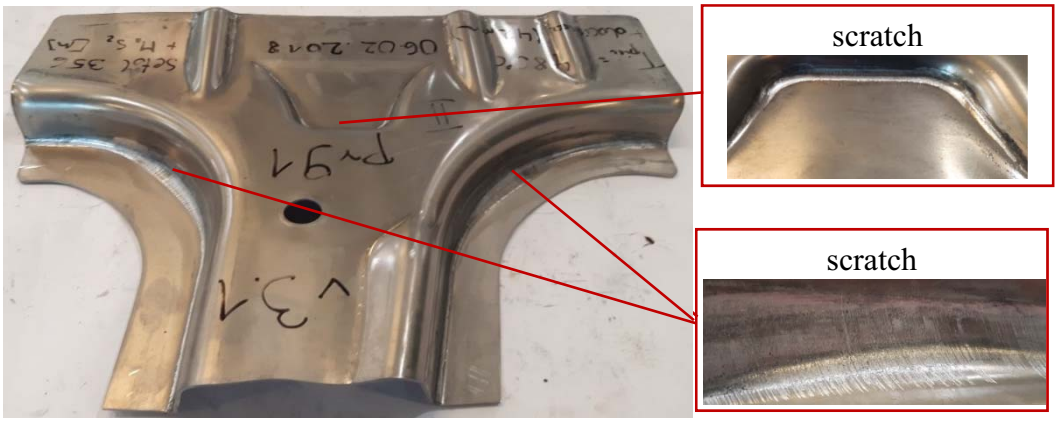

Fig. 5. Forming tests conducted with the use of Setol 356 oil mixed with molybdenum disulfide MoS_2 (lubrication of the tools only)

tests, molybdenum disulfide MoS_2 in the form of powder was added to Setol 356 to form a homogeneous suspension. According to the literature MoS_2 powder reduces friction between the working surfaces. The drawpiece, after lubricating only the tools, had no cracks, but only scratches as shown in Figure 5. Testing with the use of the graphite suspended in the water had a similar effect – the drawpiece had only slight scratches on the surfaces, mainly on the lateral surfaces.

Both of the drawpieces made with the use of setol+MoS_2 as well as with the use of the graphite did not pass the corrosion resistance tests. This is most likely due to the penetration of the graphite particles into the material and the fact that sulfur contributes to the aggressive, accelerated corrosion of the material. It was concluded that the use of both lubricants adversely affects the corrosion resistance of the samples, but significantly improves the forming conditions. The drawpieces were characterized by a very large delamination width of KTL coatings. It is probably connected with the impossibility of complete removal of the graphite layer and molybdenum disulfide from the surface of the samples after forming. Only Setol 356 passed the anticorrosion tests and therefore the Setol 356 lubricant without any additives was used for further tests. In the next stage of the study, a change in the pressure of the upper blankholder was planned. The values of 50, 30, and then 5 bar was tested. The changes in the pressure of the upper blankholder allowed to obtain the drawpiece without defects in the form of cracks. However, no significant improvement in the quality of the drawpieces' surface was achieved.

After the tests, the drawpieces were aged for 8 hours at 120°C and then their basic strength parameters were determined. The critical points from which the samples were taken for tensile and hardness tests were depicted in Fig. 6.

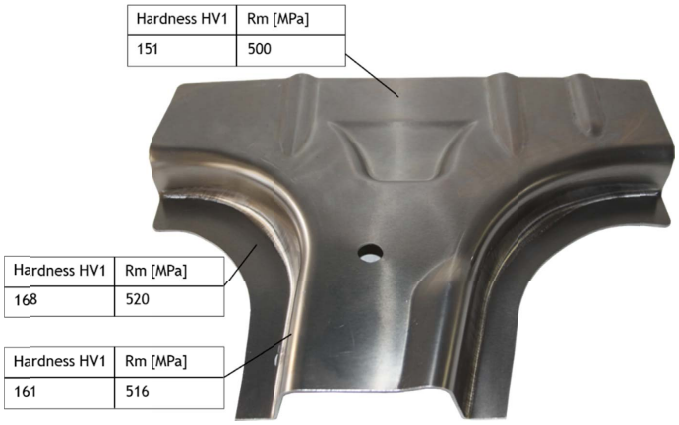

Fig. 6. Strength properties of the lower part of the B-pillar (process without the participation of the lower blankholder in the forming process, as presented in Fig. 3)

The tests prove that obtained properties are not close to the properties of T6 temper, so in the subsequent tests the lower blankholder was additionally activated. This is a component of the stamping die which is in contact with the hot blank before the start of the forming process. The use of a lower blankholder leads to the shift of the time when material cooling was started, which results in an increase in the cooling rate. Tests were carried out for different settings of the initial position of the lower blankholder as presented in Fig. 7.

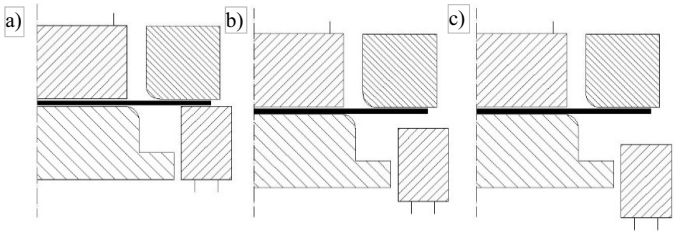

Fig. 7. Configuration of tool positions – lower blankholder a) 31 mm, b) 21 mm, c) 11 mm

Activation of the lower blankholder increased the hardness and strength of the material (Fig. 8). It was additionally noted that its height settings had an impact on the geometry of the final product.

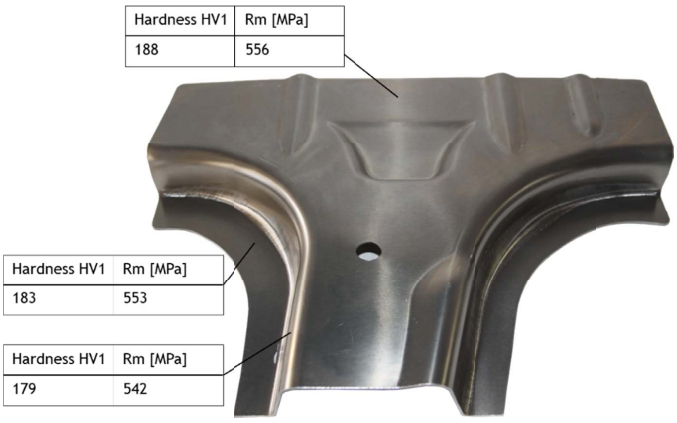

Fig. 8. Strength properties of the drawpiece made with the use of a lower blankholder (tool configuration presented in Fig. 7a)

Comparison of the numerical model and the actual geometry of the drawpiece and the changes in the thickness of the sheet metal that occurred as a result of the change of the height of the lower blankholder is shown in Figures 9 to 12 and in Table 4. Strong thinning in the case of the blankholder height equal to 21 mm results from a crack caused by a hole made for the installation of the thermocouple in order to control the temperature during heating of the input.

The measurements prove that a change in the height of the lower blankholder in the range from 0 to 31 mm significantly affects the cooling speed of the formed sheet, which results in a change in the position of the strain concentration. Additionally, due to the temperature change of the formed sheet, the coefficient of friction is changed, which results in different material thinning. Table 5 presents the results of the numerical simulation for the settings of the lower blankholder in the position of 0, 11, 21 and 31 mm, showing the strain changes at the determined points, while in Figure 13 an example of the strain contour lines for the sample formed with the lower blankholder in position "0 mm" is presented.

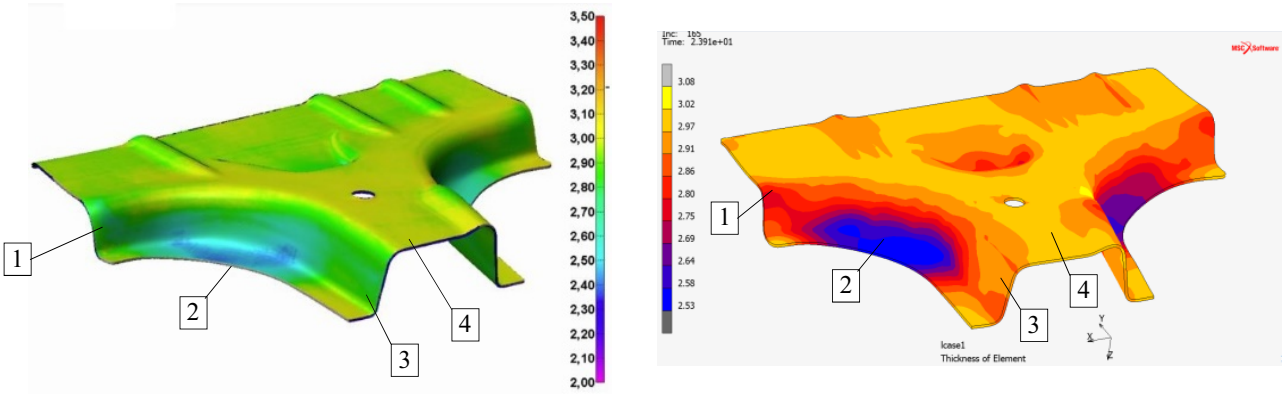

Fig. 9. Comparison of thickness for the numerical model the and actual geometry of the drawpiece (height of the lower blankholder 0 mm)

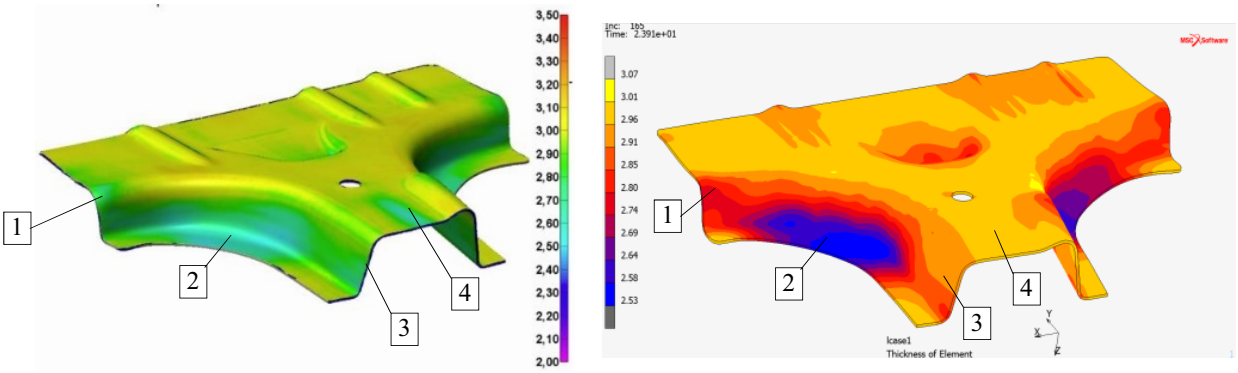

Fig. 10. Comparison of thickness for the numerical model the and actual geometry of the drawpiece (height of the lower blankholder 11 mm)

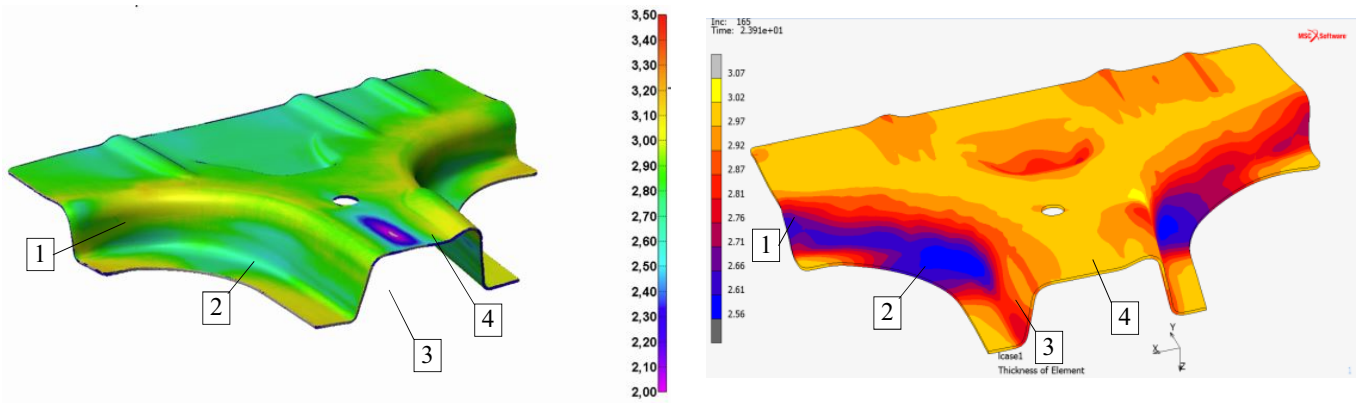

Fig. 11. Comparison of thickness for the numerical model the and actual geometry of the drawpiece (height of the lower blankholder 21 mm)

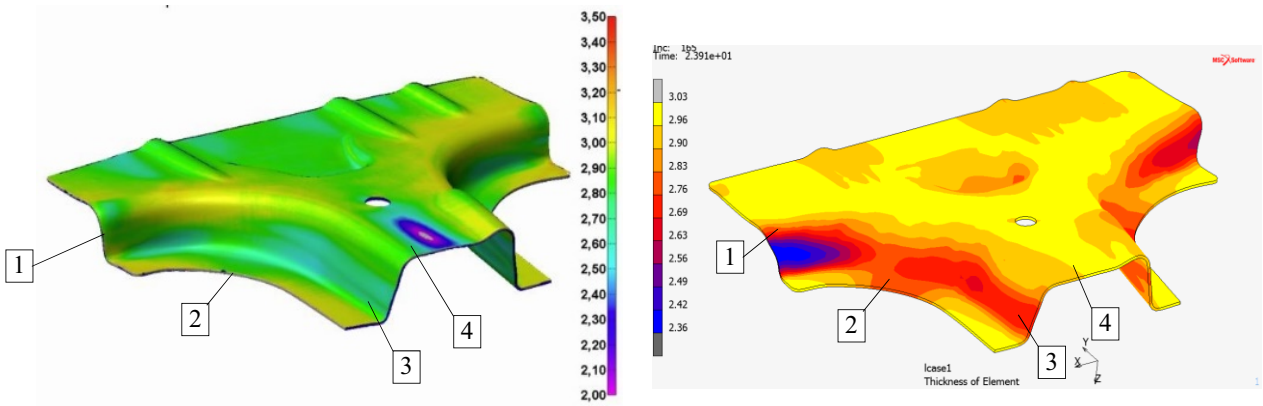

Fig. 12. Comparison of thickness for the numerical model the and actual geometry of the drawpiece (height of the lower blankholder 31 mm)

TABLE 4

Comparison of the thickness changes for the different setting of the blankholder height

Height of the lower blankholder	Measuring method	Pt 1	Pt 2	Pt 3	Pt 4
0 mm	Thickness gauge	2,90	2,32	2,84	2,98
	Scanner	2,78	2,45	2,90	3,02
	MES	2,78	2,54	2,90	2,97
11 mm	Thickness gauge	2,72	2,60	2,76	2,57
	Scanner	2,82	2,56	2,73	2,44
	MES	2,77	2,55	2,88	2,97
21 mm	Thickness gauge	2,84	2,75	2,80	2,02
	Scanner	2,80	2,70	2,80	2,00
	MES	2,67	2,61	2,79	2,97
31 mm	Thickness gauge	2,74	2,80	2,68	2,72
	Scanner	2,77	2,77	2,70	2,60
	MES	2,41	2,77	2,74	2,97

5. Summary

In order to obtain high-performance elements formed from the 7075-T6 aluminum alloy sheets, it is necessary to soften the material to a solutionized state. The solutionization process can be combined with the forming process by stamping the pre-heated blank on cold forming tools. In the presented design of the tools for stamping the lower part of the B-pillar, the upper and lower blankholders were additionally used. Due to the risk of loss of stability, the pressure of the upper blankholder should be set in the range from 30 to 50 bar and the lower blankholder to a minimum value of 5 bar. In addition to the correct geometry, attention must be paid to the strength properties of the final product, which in this case will be maximised if the lower blankholder's initial position is correct. This will result in the rapid cooling of the material, retaining the solutionized state, which is the basis for the subsequent process of artificial ageing. On the basis of the carried measurements, it can be concluded that the change in the height of the lower blankholder in the range from 0 to 31 mm results in the change in the position of the strain concentration from the flange to the sidewall due to the faster cooling at the flange.

Proper forming conditions with lubricating only the tools' surface were achieved with pure Setol 356 oil. When using a mixture of Setol 356 with molybdenum disulfide or graphite suspension, cleaning of the surface is very difficult and requires additional mechanical methods and it also reduces the corrosion resistance of the material.

The numerical model is compatible with the measurements made with the non-contact method and the thickness gauge, providing a good convergence with the real process.

Final note

Work carried out within the framework of project NCBiR, POIR.04.01.04-00-00-0088/15 "Development of the technology of pressing a B-pillar from 7xxx aluminum alloys series".

TABLE 5

Changes in total equivalent strain for the height of lower blankholder equal to 0, 11, 21, 31 mm (FEM simulation)

Height of the lower blanholder		0 mm	11 mm	21 mm	31 mm
total equivalent strain top layer	Point 1	0,212	0,214	0,296	0,545
total equivalent strain bottom layer		0,150	0,165	0,255	0,540
total equivalent strain top layer	Point 2	0,292	0,280	0,234	0,128
total equivalent strain bottom layer		0,296	0,284	0,238	0,130
total equivalent strain top layer	Point 3	0,162	0,201	0,342	0,412
total equivalent strain bottom layer		0,154	0,162	0,257	0,330
total equivalent strain top layer	Point 4	0,005	0,005	0,005	0,005
total equivalent strain bottom layer		0,004	0,004	0,004	0,005

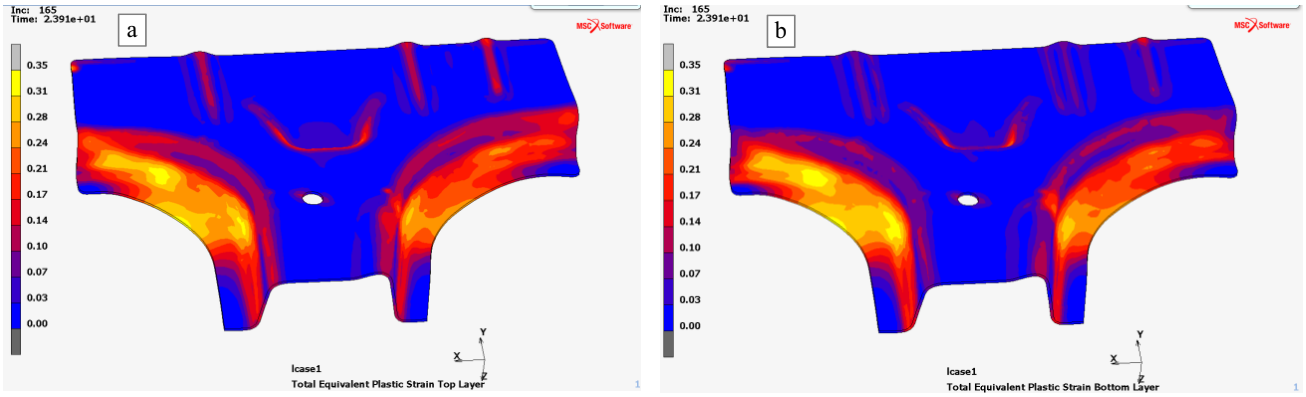

Fig. 13. Example of the strain map of two samples stamped with the lower blankholder in position "0 mm".

REFERENCES

[1] G. Winiarski, A. Gontarz, G. Samołyk, Arch. Civ. Mech. Eng. **19** (4) 1020-1028 (2019), DOI: 10.1016/j.acme.2019.05.006.

[2] A. Kubit, R. Kluz, T. Trzepieciński, D. Wydrzyński, W. Bochnowski, Arch. Civ. Mech. Eng. **18** (1) 235-244 (2018), DOI: 10.1016/j.acme.2017.07.005.

[3] D. Li, A. K. Ghosh, J. Mater. Process. Tech. **145** (3) 281-293 (2004), DOI: 10.1016/j.jmatprotec.2003.07.003.

[4] M. Kumar, N. Sotirov, C. M. Chimani, J. Mater. Process. Tech. **214** (8) 1769-1776 (2014), DOI: 10.1016/j.jmatprotec.2014.03.024.

[5] Z. Gronostajski, Z. Pater, L. Madej, A. Gontarz, L. Lisiecki, A. Lukaszek-Solek, J. Luksza, S. Mróz, Z. Muskalski, W. Muzykiewicz, M. Pietrzyk, R. E. Śliwa, J. Tomczak, S. Wiewiórowska, G. Winiarski, J. Zasadzinski, S. Ziólkiewicz, Arch. Civ. Mech. Eng. **19** (3) 898-941 (2019), DOI: 10.1016/j.acme.2019.04.005.

[6] S. Mahabunphachai, M. Koç, Mater. Des. **31** (5) 2422-2434 (2010), DOI: 10.1016/j.matdes.2009.11.053.

[7] H. Wang, Y.B. Luo, P. Friedman, M.H. Chen, L. Gao, T. Nonferr. Metal Soc. **22** (1) 1-7 (2012), DOI: 10.1016/S1003-6326(11)61131-X.

[8] P. Snopiński, T. Tomasz, K. Matus, S. Rusz, Arch. Civ. Mech. Eng. **19**, 287-96 (2019), DOI: 10.1016/j.acme.2018.11.003.

[9] M. Kumar, M. Poletti, H.P. Degischer, Mater. Sci. Eng. A **562**, 362-370 (2013), DOI: 10.1016/j.msea.2012.10.031.

[10] S. Polak, P. Kaczyński, Z. Gronostajski, K. Jaśkiewicz, J. Krawczyk, M. Skwarski, M. Zwierzchowski, W. Chorzępa, Procedia Engineer. **207**, 2399-2404 (2017), DOI: 10.1016/j.proeng.2017.10.1015.

[11] Z. Gronostajski, S. Polak, K. Jaśkiewicz, P. Kaczyński, M. Skwarski, J. Krawczyk, W. Chorzępa, K. Śliz, S. Uzar, Procedia Manuf. **27**, 98-103 (2019), DOI: 10.1016/j.promfg.2018.12.050.

[12] L. Deng, X. Wang, J. Jin, L. Xia, Procedia Engineer. **207**, 2388-2393 (2017), DOI: 10.1016/j.proeng.2017.10.1013.

[13] N. Wang, A. Ilinich, M. Chen, G. Luckey, G. D'Amours, Int. J. Mech. Sci. **151**, 444-460 (2019), DOI: 10.1016/j.ijmecsci.2018.12.002.

[14] V.M. Simões, M.C. Oliveira, H. Laurent, L.F. Menezes, J. Manuf. Process. **38**, 266-278 (2019), DOI: 10.1016/j.jmapro.2019.01.020.

[15] K. Zhao, D. Ren, B. Wang, Y. Chang, Int. J. Heat Mass Transf. **132**, 293-300 (2019), DOI: 10.1016/j.ijheatmasstransfer.2018.11.158.

[16] P. Chen, Z.Q. Lin, G.L. Chen, K. Muammer, T. Nonferr. Metal Soc. **16** (2) 267-273 (2006), DOI: 10.1016/S1003-6326(06)60045-9.

[17] E. Evangelista, A. Forcellese, F. Gabrielli, P. Mengucci, J. Mater. Process. Tech. **24**, 323-332 (1990), DOI: 10.1016/0924-0136(90)90193-X.

[18] P. Cavaliere, J. Light Met., **2** (4), 247-252 (2002), DOI: 10.1016/S1471-5317(03)00008-7.

[19] A. B. Barenji, A. R. Eivani, M. Hasheminiasari, H. R. Jafarian, J Mater. Res. Tech. **1160**, 1-15 (2019), DOI: 10.1016/j.jmrt.2019.11.092.

[20] X. Fan, Z. He, S. Yuan, P. Lin, Mater. Sci. Eng **587**, 221-227 (2013), DOI: 10.1016/j.msea.2013.08.059.

[21] N.R. Harrison, S.G. Luckey, SAE Int. J. Mater. Man. **7** (3) 567-573 (2014), DOI: 10.4271/2014-01-0981.

[22] B.A. Behrens, F. Nürnberger, C. Bonk, S. Hübner, S. Behrens, H. Vogt, J. Phys. Conf. Ser. **896** (1) 012004 (2017), DOI: 10.1088/1742-6596/896/1/012004.

[23] A. Foster, T. Dean, J. Lin, European Patent Specification WO 2010/032002, **1** (19) 1-11 (2013).

[24] S.D. Mackenzie, J. Newkirk, Proc. 8th Semin. IFHTSE, Dubrovnik **119**, (2001).

[25] W.S. Mattos, G.E. Totten, L.C.F. Canale, ASM Handbook, ASM International **4E**, 148-178 (2016), DOI: 10.1520/MPC20160125.

[26] W.-C. Xiao, B.-Y. Wang, Y. Kang, W.-P. Ma, X.-F. Tang, Rare Met. **36** (6) 485-493 (2017), DOI: 10.1007/s12598-017-0919-4.

[27] P. Priya, D.R. Johnson, M.J.M. Krane, Comp. Mater. Sci. **139**, 273-284 (2017), DOI: 10.1016/j.commatsci.2017.08.008.

[28] L. Hadjadj, R. Amira, D. Hamana, A. Mosbah, J. Alloy. Compd. **462**, 279-283 (2008), DOI: 10.1016/j.jallcom.2007.08.016.

[29] K. Zheng, Y. Dong, J. Zheng, A. Foster, J. Lin, H. Dong, T.A. Dean, Mater. Sci. Eng. **761**, 138017 (2019), DOI: 10.1016/j.msea.2019.06.027.

[30] Y. Liu, Z. Zhu, Z. Wang, B. Zhu, Y. Wang, Y. Zhang, Procedia Engineer. **207**, 723-728 (2017), DOI: 10.1016/j.proeng.2017.10.819.

[31] E. Scharifi, R. Knoth, U. Weidig, Procedia Manuf. **29**, 481-489 (2019), DOI: 10.1016/j.promfg.2019.02.165.

[32] J. Zhou, B.Y. Wang, J.G. Lin, L. Fu, W.Y. Ma, T. Nonferr. Metal Soc. **24** (11) 3611-3620 (2014), DOI: 10.1016/S1003-6326(14)63506-8.

[33] J. Jang, J. Lee, B. Joo, Y. Moon, T. Nonferr. Metal Soc. **19** (4) 913-916 (2009), DOI: 10.1016/S1003-6326(08)60376-3.

[34] S. Narayan, A. Rajeshkannan, J. Mater. Res. Tech. **6** (2) 101-107 (2017), DOI: 10.1016/j.jmrt.2016.03.012.

[35] K. Omer, C. Butcher, M. Worswick, Int. J. Mech. Sci. **165**, 105218 (2020), DOI: 10.1016/j.ijmecsci.2019.105218.

[36] J. Lu, Y. Song, L. Hua, K. Zheng, D. Dai, J. Alloy. Compd. **767**, 856-869 (2018), DOI: 10.1016/j.jallcom.2018.07.173.

[37] Y. Song, D. Dai, P. Geng, L. Hua, Procedia Engineer. **207**, 741-746 (2017), DOI: 10.1016/j.proeng.2017.10.822.

[38] A.R. Riahi, A.T. Alpas, Surf. Coat. Tech. **202** (4-7) 1055-1061 (2007), DOI: 10.1016/j.surfcoat.2007.07.085.

[39] Y. Dong, K. Zheng, J. Fernandez, X. Li, H. Dong, J. Lin, J. Mater. Process. Tech. **240**, 190-199 (2017), DOI: 10.1016/j.jmatprotec.2016.09.023.

[40] M. Vrolijk, D. Lorenz, H. Porzner, M. Holecek, Procedia Engineer. **183**, 336-342 (2017), DOI: 10.1016/j.proeng.2017.04.049.

[41] X. Liu, O. Fakir, Z. Cai, B. Dalkaya, K. Wang, M.M. Gharbi, L. Wang, J. Mater. Process. Tech. **273**, 116245 (2019), DOI: 10.1016/j.jmatprotec.2019.05.026.

[42] H. Li, Z. Hu, Y. Chen, Q. Sun, X. Zhou, Int. J. Light. Mater. Manuf., (2019), DOI: 10.1016/j.ijlmm.2019.12.004.